Biochemistry and Biophysics Reports 42 (2025) 102036

Contents lists available at ScienceDirect

Biochemistry and Biophysics Reports

journal homepage: www.elsevier.com/locate/bbrep

Porcine intestinal organoids cultured in an organ-on-a-chip microphysiological system

James Bacon, Halie Kitchel, John Stutz, Jack Hua Chen, Aaron Smith, Robert D. Van Horn, Christopher Moreland, Trent Abraham, Thomas Baker [*,1], Eitaro Aihara, Kathleen Hillgren

Eli Lilly and Company, Lilly Corporate Center, Indianapolis, IN, 46285, USA

A B S T R A C T

Preclinical studies are a vital component of pharmaceutical development and improvements in the predictive value of in vitro studies are essential. Organ-on-a-chip in vitro models are a recent advancement in the pursuit of improved reproduction of in vivo tissue complexity. Here, we report the development and characterization of porcine intestinal cells from organoids on chips with microfluid dynamics and peristaltic-like strain in a microphysiological system. Intestinal epithelial cells were grown on a porous membrane as a co-culture with human intestinal microvascular endothelial cells for up to 12 days. These cultures formed villi-like structures and established a tight barrier replete with F-actin and tight junctions. A demarcated region of the epithelial cells was in an actively proliferative stage, reminiscent of intestinal crypts. The intestinal epithelial cell growth was characterized for the presence of enterocytes, goblet cells and enteroendocrine cells. Notable drug transporters and CYP450 metabolic activity were present in these cultures. The organoid chip maintained barrier function as the paracellular permeability was low. In contrast, the permeability enhancer, sodium caprate (C_{10}), increased the apparent permeability of molecular weight marker compounds by 2- to 3-fold, and upon removal of C_{10}, the barrier was shown to be recovered. The porcine intestinal chip represents a new in vitro model with potential application in multiple aspects of pharmaceutical testing including drug metabolism, drug transporters and safety.

1. Introduction

The identification of Lgr5-positive cells from intestinal crypts and subsequent determination that these were stem cells, introduced new possibilities to recapitulate organs in vitro through the application of organoid research [1]. The identification of these stem cells was soon followed by the successful establishment of cultured intestinal organoids [2]. The organoids retained the ability to generate cellular components and functions similar to in vivo intestinal epithelium. In a relatively short period of time, intestinal organoids have been isolated and cultured successfully from numerous species including dogs, cats, cattle, chickens [3–5], as well as porcine [6–8].

The field of organoids created new avenues for enhanced in vitro gut models and the potential use in preclinical pharmaceutical testing in areas including drug permeability, transport, metabolism and toxicology, as well as utility in the replacement, reduction and refinement (3Rs) of animal research. However, initial iterations of organoid research were not readily amenable for a broad spectrum of pharmaceutical testing applications. Experimentation required for preclinical drug development was limited by procedural constraints since intestinal organoid cultures were established in 3D and embedded in Matrigel. The organoids were grown as spheres which conformed to a reversed orientation relative to the intestine, with the luminal compartment toward the interior of the sphere and the basolateral surface facing outward. This proved to be an inefficient configuration for many testing purposes. The development of 2D intestinal organoid cultures grown on Transwells significantly enhanced the testing paradigm [9]. This was followed by 2D models established in various species [10,11] including porcine [12]. The continued progress of adapting intestinal organoids towards more effective in vitro models merged with the development of microphysiological systems (MPS), or organ-on-a-chip technology.

MPS technology utilize microfluidics, mechanical stress and tissue-tissue interfaces in hollow channels to more faithfully replicate in vivo systems. This was applied to an intestinal model using the human colorectal cancer cell line, Caco-2, grown on fabricated microfluidic devices [13]. The dynamic stress and laminar flow present in this in vitro 'gut chip' induced changes in the epithelium not observed in static Transwell cultures [14]. More recently, human duodenum organoids were grown in an organ chip microfluidic format in which the epithelial cell growth bore striking resemblance to intestinal tissue [15]. However, despite the rapid advancement in the field of organoids and MPS technology, the number of well-characterized organoid-based MPS intestine

* Corresponding author.
E-mail address: baker_thomas_k@lilly.com (T. Baker).
[1] Lead contact.

https://doi.org/10.1016/j.bbrep.2025.102036
Received 24 February 2025; Received in revised form 16 April 2025; Accepted 25 April 2025

models have generally been limited.

The use of porcine as a non-rodent species in preclinical pharmaceutical testing has been receiving greater attention [16,17]. Porcine and humans have similar digestive metabolic profiles, anatomical compositions, are omnivorous and have a comparable genomic sequence. These shared similarities to humans make them an attractive species to conduct pharmaceutical research [18]; [19]). Comparisons to humans include aspects of the gut which may serve as a useful tool to assess molecule permeability.

Most 2D in vitro gut models lack the complexity of intestinal tissue and are limited in their morphogenic differentiation that occurs in vivo. The mucosal layer is insufficient in many traditional in vitro models as well, as is the ability to adequately express transporters and metabolizing enzymes, all of which are needed to recapitulate the intestine. Mechanistic preclinical studies conducted in traditional intestinal models may not adequately reflect in vivo response, and therefore may result in an erroneous in vitro to in vivo extrapolations (IVIVE) [20]. In addition, increased interest in permeation enhancement for peptide therapeutics may also be inadequately tested with most traditional in vitro cell-based gut models, particularly as it relates to barrier recovery upon removal of permeability enhancer treatment [21]. Porcine intestinal organoids cultured in a microfluidic system have the potential to recapitulate intestinal tissue and functional elements that traditional in vitro systems have difficulty achieving and are an attractive alternative to many existing gut models. With the relative ease of porcine organoid isolation, growth and maintenance in culture, as well as ready tissue availability, they represent a useful addition for preclinical pharmaceutical research.

This paper describes the characterization of the porcine jejunum organoid in an MPS format, for differentiation, permeability, transport, metabolism and permeability enhancement.

2. Methods

2.1. Pig intestinal organoid cultures in a chip device

Jejunum intestinal organoids were established according to a previously described protocol [12]. Crypts from male Gottingen minipig jejunum were previously isolated and cryopreserved [22]. Animal experiments were conducted with the full ethical and regulatory compliance requirements with the Covance Laboratories IACUC (International Animal Care and Use Committee) guidelines and expectations for animal care and use/ethics. Frozen stocks of intestinal organoids were recovered and suspended in Matrigel (Corning) and cultured in human IntestiCult Organoid growth medium (Stemcell Technologies) at 37 °C/5 % CO_2 and 100 μg/mL of primocin (InvivoGen). These 3D organoids cultures were grown for 7 days, then harvested and dissociated into a suspension comprised of fragments and single cells. The suspension media consisted of IntestiCult OGM medium, 100 μg/mL primocin, 10 μM Y-27632 (Stemcell Technologies) and 5 μM CHIR99021 (Reprocell).

The chips used to support the epithelial and endothelial cell growth were obtained from Emulate, Inc. (Boston, MA). The design details of the polydimethylsiloxane (PDMS) chips are described previously [15]. An extracellular matrix (EM) was applied to the top and bottom channels of chips. The top channel EM consisted of 100 μg/mL Matrigel and 200 μg/mL Type I collagen (Corning) while the bottom channel EM was composed of 200 μg/mL type IV collagen (Sigma) and 30 μg/mL fibronectin (Corning). The EM was added to the appropriate channel according to Emulate protocol and allowed to incubate at 37 °C/5 % CO_2 for 2–3 h. The channels were washed with complete medium prior to addition of organoid fragments. The suspension of dissociated organoids was counted and adjusted to ~10-15 × 10^6 cells/mL. The top channel of the chips was seeded with 35 μL of the cell suspension and incubated undisturbed overnight. The following day the channel was washed with degassed, complete medium and the flow within the chips was initiated at 30 μL/h for the duration of the culturing. On day 3 post-seeding, Y-27632 and CHIR were removed from the medium for the remainder of the time in culture. The bottom channel endothelial cells were seeded into chips on day 7. Human Intestinal Microvascular Endothelial Cells (HIMECs, ScienCell) were expanded in 75 cm^2 flasks prior to seeding into chips. HIMECs were cultured in Endothelial Cell Basal Medium-MV2 Supplement Pack (PromoCell) and at the time of seeding, suspended at approximately 8 × 10^6 cells/ml. The bottom channel was seeded with 15 μL of cell suspension and allowed to attach under static conditions with the chips inverted for 1 h at 37 °C/5 % CO_2. Chips were then restored to the upright orientation and flow was resumed for both channels at 30 μL/h. A 2 % peristalsis-like stretch was applied to the chips on day 7, which was increased to 10 % on day 8 and continued throughout the remainder of the study.

2.2. Permeability assessment

The apparent paracellular permeability (P_{app}), which describes the flux of a molecule crossing from the epithelial to the endothelial compartments, was calculated using the fluorescent markers Lucifer Yellow (450 Da) and Cascade Blue Dextran (3 kDa). Lucifer Yellow (25 μM) and dextran (50 μM) were added to medium in the top channel epithelium inlet reservoir and monitored for diffusion into the bottom channel endothelium effluent. Concentrations of Lucifer Yellow and 3 kDa dextran in top and bottom reservoirs were quantified using an 8-point standard curve with the resulting P_{app} value calculated according to the following formula:

$$Papp\left(\frac{cm}{s}\right) = \frac{Coutput\ \ (\mu M)^{*}Flow\ rate\left(\frac{mL}{s}\right)}{Cinput(\mu M)^{*}A\ (cm2)}$$

Where C_{output} is the concentration in the receiver endothelial compartment, C_{input} is the concentration in epithelial donor compartment and A is the seeded area. Permeability was measured during multiple studies and for varied lengths of time in culture in order to establish a baseline standard.

In some cases, permeability change was assessed in the presence of sodium caprate (C_{10}), permeation enhancer (PE). Jejunum chips were cultured for 8–9 days prior to initiating C_{10} PE studies using the paracellular markers, Lucifer Yellow (25 μM) and 3 kDa dextran (50 μM). The optimal day in culture to begin studies was determined by morphological inspection of chips via phase contrast microscopy. The P_{app} values were monitored at least 24 h prior to the onset of the study to ensure the intestine chips had established a tight barrier. C_{10} was tested at concentrations of 5, 10 and 25 mM. Duplicate chips for each study were treated with varying concentrations of C_{10} added to media containing Lucifer Yellow and 3 kDa dextran in the top channel donor reservoir. The C_{10}-treated chips and paired control chips were dosed for 90 min at the standard flow rate of 30 μL/h. At the conclusion of the 90 min treatment, the dosing solutions were removed and replaced with media supplemented with Lucifer Yellow and 3 kDa dextran. The flow rate of the chips was increased to 50 μL/h which afforded a greater volume of sample collected at early timepoints, enabling an accurate calculation of P_{app} values. At 2 and 4 h posttreatment, the total volume of media in the top and bottom outlet reservoir was removed for Lucifer Yellow and 3 kDa dextran quantification. After the 4 h sample collection, the flow rate was reduced to 30 μL/h per Emulate, Inc. standard condition recommendation. Media samples were collected from the top and bottom channel reservoirs at 24 and 48 h posttreatment. Lucifer Yellow and 3 kDa dextran were quantified for each timepoint collected and used to determine P_{app} values.

2.3. Morphology and cell type analysis

Intestine chips were fixed with 4 % formaldehyde or methanol and

permeabilized with 0.1 % (vol/vol) Triton X-100/5 % (wt/vol) goat serum prior to overnight incubation with primary antibodies. Goat serum was used for blocking fixed tissues. Primary antibodies were directed against zonula occludins (ZO-1, rabbit monoclonal, Abcam), Ki-67 (rabbit polyclonal, Abcam), villin (rabbit monoclonal, Abcam), chromogranin A (CHGA, rabbit polyclonal, Abcam), P-glycoprotein (P-gp, mouse monoclonal, Invitrogen), Trefoil factor 3 (TFF3, rabbit monoclonal, Thermo), E-Cadherin (mouse monoclonal, BD Transduction Lab) and mucin 2 (MUC2, rabbit polyclonal, GeneTex). F-actin was identified using an Alex Fluor 488 phalloidin conjugate (Life Technologies) and 5-ethynyl-2′-deoxyuridine (EdU) incorporation was conducted using a Click-iT EdU Imaging Kit (Invitrogen). Immunofluorescent (IF) images were taken using a LSM880 (Zeiss) or Opera Phenix (PerkinElmer). Media levels of citrulline were quantified in the top channel outlet reservoir by LC/MS methods.

2.4. Gene expression assessment

Total RNA was isolated from the top channel of intestine chips using Direct-Zol RNA MiniPrep (Zymo Research) or PureLink Mini Kit (Thermo Fisher Scientific). Total isolated RNA was configured using the Nanodrop 8000 Spectrophotometer (Thermo Scientific) and transcribed to cDNA using high-capacity cDNA reverse transcription kit (Applied Biosystems) and SUPERase-ln Rnase Inhibitor (Invitrogen). cDNA was run through a Veriti 96-well Thermal Cycler (Applied Biosystems) for ~135 min. TaqMan Gene Expression Master Mix (Applied Biosystems) was used in all assays. The qRT-PCR was performed using the Viia7 Real-Time PCR System (Applied Biosystems) and TaqMan Gene Expression Assays (Applied Biosystems) were used to probe for the following genes: leucine-rich-repeat-containing G-protein-couple receptor 5 (LGR5, Ss04955120_g1), mucin 2 (MUC2, Ss03377386_u1), proliferating cell nuclear antigen (PCNA, Ss03377029_g1), sodium/glucose cotransporter 1 (SGLT1, Ss03374377_m1), villin (Ss06886976_m1), lysozyme (LYZ, Ss03394856_m1), chromogranin A (CHGA, Ss03374348_m1), P-glycoprotein (P-gp, Ss03373435_m1), peptide transporter 1 (PEPT1, Ss03394774_m1) and glyceraldehyde-3-phosphate dehydrogenase (GAPDH, Ss03374854_g1). Gene expression was measured in duplicate chips from a single study to evaluate intra-study variability, and in an intestine chip from a separate study to assess inter-study expression. The cycle threshold (Ct) was determined for each sample. The relative gene expression comparison was made to GAPDH Ct values and expressed as a ratio of GAPDH Ct/gene of interest (GOI) Ct.

2.5. Drug transporter activity

BCRP and P-gp function were evaluated by live cell imaging of Day 9 intestine chips with the fluorescent substrates, BODIPY-prazosin and rhodamine 123, respectively (Sigma). Briefly, for BCRP chips were pretreated with 20 μM chrysin (Sigma), an inhibitor of BCRP, or vehicle for 1hr, followed by 2 h cotreatment with 5 μM BODIPY-prazosin. Chips were then washed with DPBS and the top channel epithelium was immediately imaged by fluorescence microscopy (details to follow). For P-gp, cultures were pretreated with 2.5 μM LSN335984 (Eli Lilly and Co.), an inhibitor of P-gp, or vehicle for 30 min followed by cotreatment with 10 μM rhodamine 123. Chips were washed and then imaged by fluorescence microscopy.

Transporter function was also assessed for P-gp and PEPT1 by measuring the movement of substrates from the top channel to the bottom channel. For P-gp, Day 10 chips were perfused with the 100 nM vincristine, with or without the P-gp inhibitor, LSN335984 (5 μM). For PEPT1, a separate set of chips were treated with 100 μM cefadroxil (Sigma) in the absence or presence of 100 μM losartan (Sigma), an inhibitor of PEPT1. For both drug transporters, intestine chips were treated for 3 h after which samples were withdrawn from the top and bottom donor and receiver reservoirs. Substrates (vincristine and cefadroxil) were quantified by LC/MS methods (details). The total protein amounts were determined for each chip and the results were normalized to pmol/mg protein.

2.6. Induction of CYP3A activity

Jejunum intestine chips (Day 8) were pretreated with 20 μM rifampicin (Sigma) or 0.1 % DMSO for 48 h as a means of inducing porcine CYP3A activity. Following the pretreatment, 50 μM testosterone (Sigma-Aldrich) was added as a cotreatment with rifampicin or to the DMSO control chips. Samples were withdrawn at 4 and 24 h from the top and bottom channel donor and receiver chambers and then quenched with acetonitrile. The formation of 6β-hydroxytestosterone was determined by LC/MS/MS. Total protein amounts were determined for each chip and the results were normalized to pmol/mg protein.

3. Results

3.1. Porcine jejunum MPS culture growth

As previously described, organoid fragments were applied to the top microchannel of a two-channel (top/luminal and bottom/vascular) microfluidic hollow chamber (Fig. 1A). Jejunum organoids, grown as 3D cultures (Fig. 1B), were harvested and seeded as a mixture of single cells and partially intact organoid fragments (Fig. 1C). The growth progression to fully formed jejunum chip cultures was largely independent of the precise composition of single cells and fragments. Seeded cells formed monolayers within 24 h of seeding (Fig. 1D), after which media flow was initiated at 30 μL/h. Previous reports with gut chips have emphasized the importance of including physiological fluid flow of fresh cell culture media, a peristaltic-like stretch and the addition of endothelial cells (HIMEC) to the bottom vascular channel [15,23]. Similar conditions were applied to the intestine chip studies reported here. The addition of HIMECs on Day 7 (Fig. 1E), as well as a peristaltic stretch (2 %), were an inflection point for inducing noticeable changes in organ chip morphology. By Day 9 (Fig. 1F), cultures established well-defined clefts, three-dimensional morphology and a cuboidal epithelial appearance. Differential interference contrast (DIC) microscopy images highlight the topographical features of the epithelial growth (Fig. 1G).

Furthermore, as shown in Fig. 2, by Day 10 the cytoskeleton marker, F-actin, is extensively found along the apical boundaries throughout the villi-like projections seen in views from above (Fig. 2A) and in cross-section (Fig. 2B). Tight junctions are another feature of intestinal tissue and appeared throughout the pig jejunum MPS cultures. Fig. 2C and D shows the membrane-associated ZO-1 tight junction in views from above and in cross-section, respectively, and Fig. 2E confirm the presence of E-cadherin tight junctions in a cross-sectional view of an intestine chip.

3.2. Barrier development

The permeability of the epithelial barrier was evaluated from Day 7 to Day 10, which encompassed a timeframe that was anticipated to be optimal for initiating studies. A representative assessment is shown in Fig. 3. The drop in P_{app} values for both of the passive permeability markers, 3 kDa dextran (Fig. 3A) and Lucifer Yellow (Fig. 3B), suggested increased tightening as a function of days in culture as well as the addition of HIMECs on Day 7. The P_{app} values equilibrated at approximately Day 9 and 10. The permeabilities of 3 kDa dextran and Lucifer Yellow, at the time typical studies were conducted (Day 9 and 10), were approximately 1×10^{-7} and 4×10^{-7} cm/s, respectively. Dextran P_{app} values below 1-2 x 10^{-6} cm/s are indicative of tight epithelial barriers. Lucifer Yellow (450 Da) routinely had higher permeability values than dextran (3000 Da) which was consistent with the differences in molecular weights of the two markers. Low P_{app} values were repeatedly observed in numerous independent studies, ranging from 0.5 to 1 x 10^{-7} cm/s for 3 kDa dextran and 2-4 x 10^{-7} cm/s for Lucifer Yellow, which

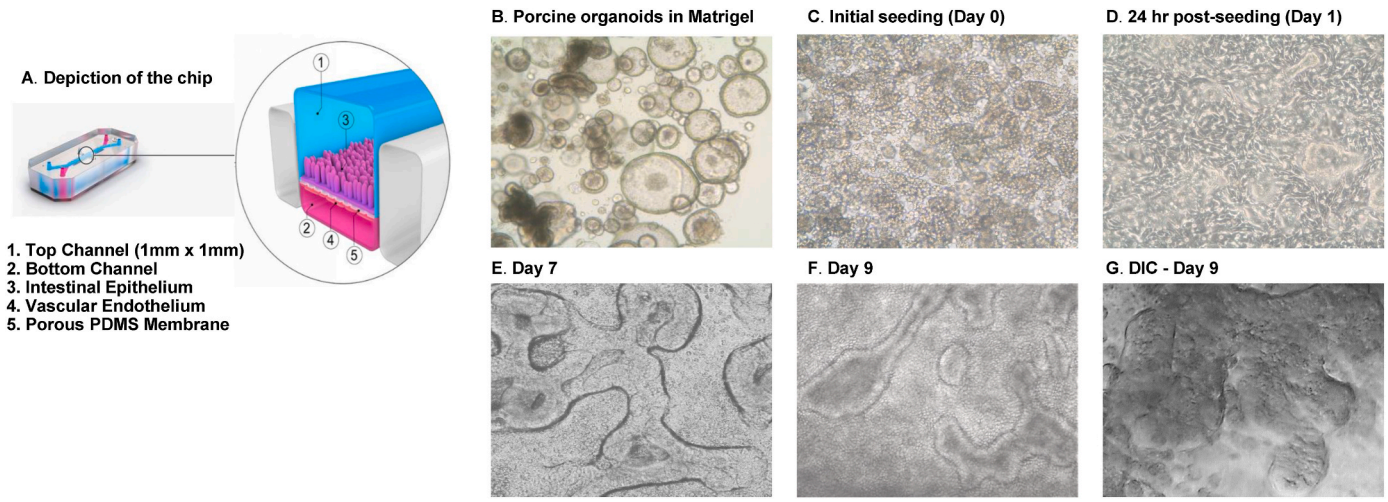

Fig. 1. Graphical representation of the chip components (panel A), 3D cultures of porcine organoids in Matrigel (panel B) and jejunum cell cultures over time (panels C–F). Phase-contrast 10X microscopy of pig jejunum organoids (panel B), harvested and immediately seeded onto chips (panel C), followed by 1 (panel D), 7 (panel E) and 9 days (panel F) in culture. DIC micrograph of jejunum cultures on Day 9 (panel G).

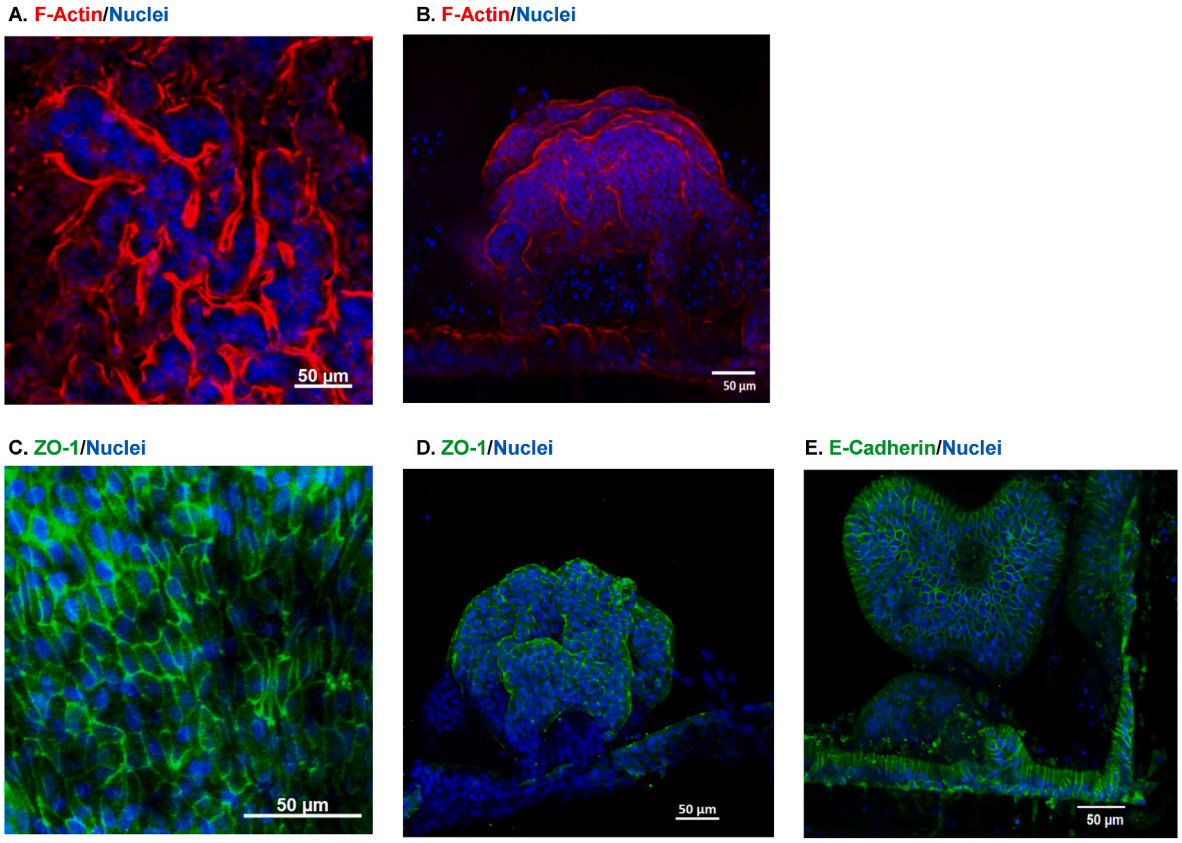

Fig. 2. Confocal immunofluorescent microscopy demonstrates structural components of porcine jejunum chips. Representative images show the presence of F-actin in Day 10 intestine chips viewed from above (panel A) and in cross-section (panel B), and the tight junction marker, ZO-1, shown from above (panel C) and cross-sectional views (panel D). The tight junction marker, E-cadherin (panel E), is shown in cross-section in Day 9 cultures.

pointed to the predictable response of the jejunum MPS cultures.

3.3. Characterization of organoid morphogenesis in the jejunum MPS

To further characterize the pig jejunum chip cultures, we examined Ki-67 as a function of days in culture to ascertain both the location and extent to which cells stained positively for this proliferative marker. The cross-section images from Fig. 4A–C demonstrated that cultures in an early stage of growth, Day 4 (panel A), had a high level of Ki-67-positively labelled cells. At Day 7 (panel B) the number of cells stained for Ki-67 declined relative to Day 4, and at Day 11 (panel C), the final day in culture, Ki-67 presence was absent. The regional association of Ki-67-stained cells at Day 4 and Day 7 is predominantly in the lower portions of epithelium growth, consistent with crypt localization in vivo. The incorporation of EdU is a more specific measure of DNA synthesis. Views from above in Supplement Fig. 1 show the relative localization of

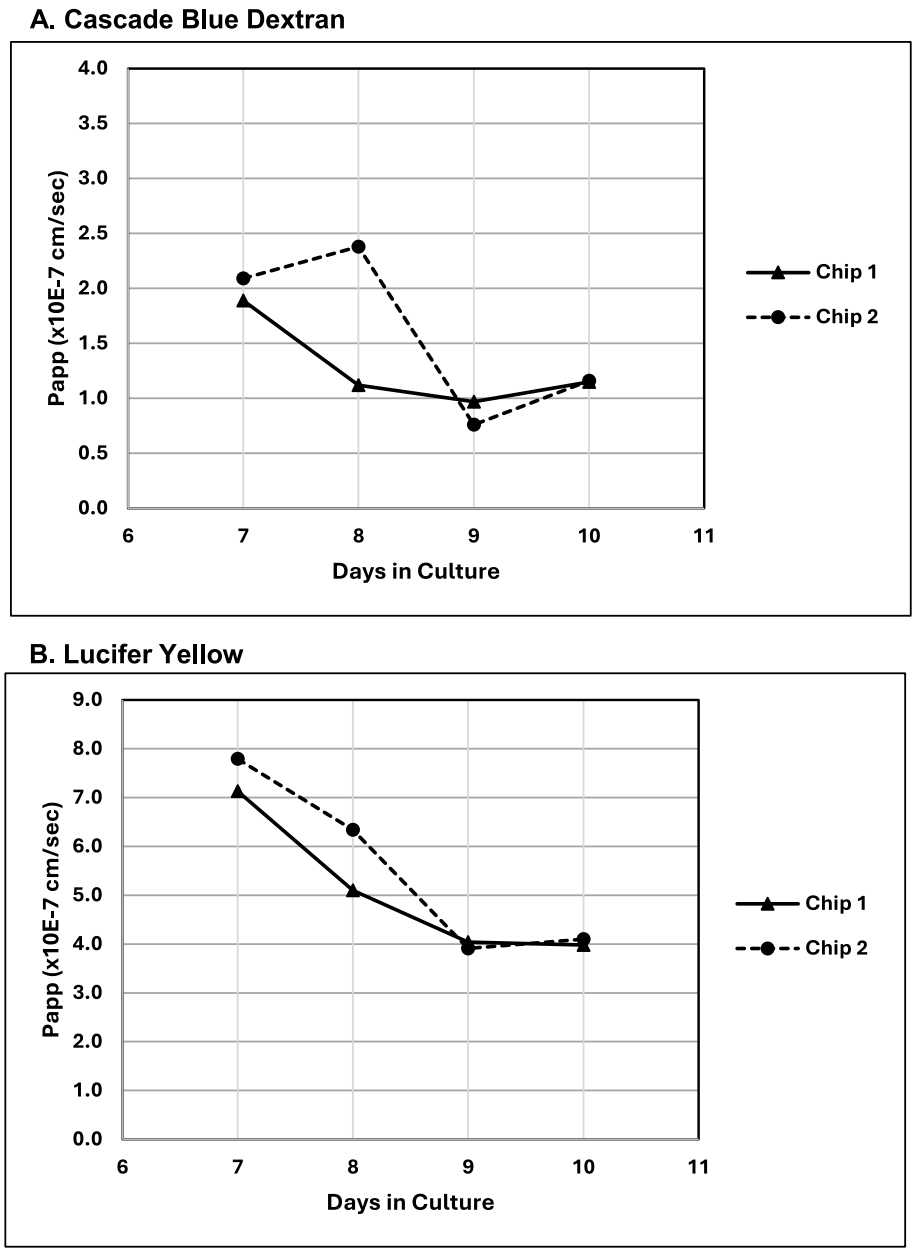

Fig. 3. Intestinal barrier function measured with fluorescent markers 3 kDa Cascade Blue dextran (panel A) and 0.4 kDa Lucifer Yellow (panel B) over time. The mean apparent permeability (P_{app}) was determined from duplicate chips (n = 2).

EdU incorporation in Day 9 intestine chips. The nuclear appearance of EdU coincided only in the lower regions of cell growth (Fig. S1A) and was absent from villi-like structures further up along the z-axis (Fig. S1B) in the intestine chips. Both the Ki-67 and EdU results suggested a crypt-like region resided closest to the porous PDMS surface.

Along with changes in the morphology of cultures and identification of crypt regions, specific markers of epithelium differentiation were also assessed. Enterocytes are the primary cell type populating the intestinal epithelium and brush border. Citrulline, an enterocyte biomarker, was quantified in the jejunum MPS as a measure of culture differentiation. The progression from Day 2 to Day 9, shown in Fig. 5, suggested an increased presence of enterocytes over time. Additional support for the presence of enterocyte differentiation is provided by detection of villin, shown in the cross-sectional IF image (Fig. 6A) and in the view from above (Fig. 6B). The cross-sectional view (6A) demonstrated an apical staining pattern of villin in the epithelial layer of the top channel and view from above (6B) showed the extent to which villin is present along the length of the intestine chip.

Goblet cells are present in far less abundance than enterocytes but play the primary role in generating an intestinal mucosal layer. One of the proteins that form the mucosa and is secreted by goblet cells is MUC2. Fig. 6C shows an IF view of MUC2 from above along the length of the intestine chip. TFF3 is another protein secreted by goblet cells and additional evidence for the differentiation of goblet cells in intestine chips is demonstrated in Fig. 6D and E showing IF staining of TFF3 *along the apical* boundary of the epithelium as well as intracellular localization to individual cells (panel D) consistent with goblet cell formation. The depth of the cross-sectional image shown in Fig. 6E is approximately 500 μm which provides greater perspective of the layering of TTF3 along the length of the intestine chip.

An additional cell type that results from fully differentiated epithelium is the appearance of enteroendocrine cells. As with goblet cells, enteroendocrine cells are few in number compared to enterocytes. Jejunum chip cultures were immunoassayed for CHGA as a marker of

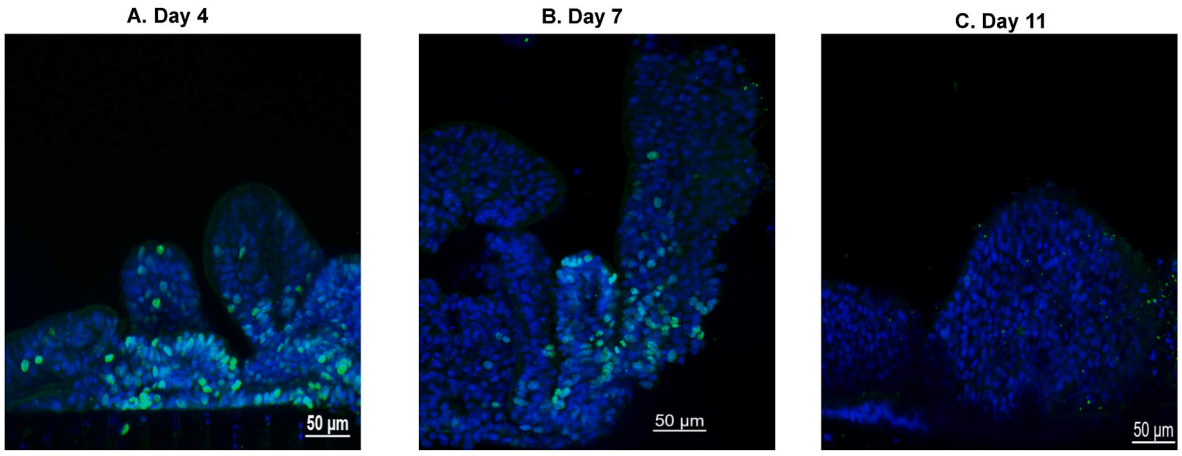

Fig. 4. Cell proliferation in jejunum chips determined by Ki-67 immunostaining. Immunofluorescent detection of Ki-67-positive staining cells (green nuclei) in cross sections of jejunum chips at day 4 (panel A), day 7 (panel B) and day 11 (panel C), showing the presence of actively cycling cells predominantly positioned in the lower region of epithelial growth, and declining in number over time.

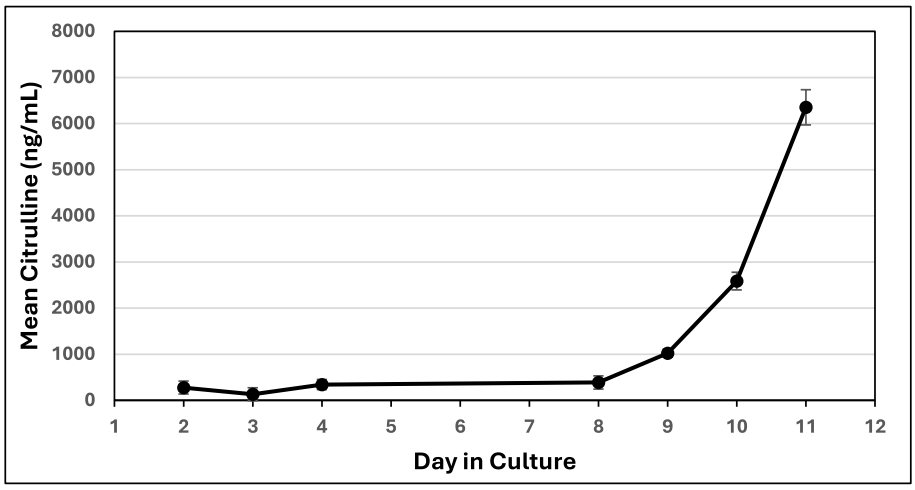

Fig. 5. Media accumulation of the enterocyte biomarker, citrulline, measured in the top channel of jejunum chips from days 2 through 11 in culture. A minimum of eight chips were measured for each timepoint. The results are background-corrected and present the mean ± standard error (n = 8–11).

enteroendocrine cells. Fig. 6F showed a characteristic intracellular localization of CHGA staining, providing additional evidence for differentiation of the intestine chip cultures.

3.4. Gene expression

A panel of nine genes were evaluated for expression by RT-qPCR and the Ct values were compared to the housekeeping gene, GAPDH. The expression profile looked at the variability between intestine chips within a single study and inter-variability across two separate studies. The relative gene expression results shown in Fig. 7 are consistent with the anticipated relative abundance of the specific cell types or intestinal characteristics associated with the genes assayed. The genes which are associated with enterocytes, SGLT1 and villin, had the largest relative expression levels and were the most similar to GAPDH, while CHGA, which is a marker for lesser abundant enteroendocrine cells, had a smaller expression ratio. Expression of MUC2, which is a goblet cell marker, also had a smaller relative expression value than enterocyte-related genes. Genes associated with the crypt included LGR5 and PCNA. Both had relative expression values substantially less than enterocyte markers, as anticipated. Similarly, the relative expression for LYZ, a Paneth cell gene product, was less than enterocyte-related genes. Two drug transporters, P-gp and PEPT1, were also included in the expression assessment. Both genes had large relative expression levels, only slightly less than the enterocyte markers which suggested the transporters are highly expressed in the intestine chips, consistent with in vivo tissue.

The intra- and inter-variability across all genes assayed was relatively low. Fig. 7 demonstrated the overall trends were comparable between the two chips within Study 1, as well as similar responses between Study 1 and Study 2.

3.5. Drug transporter function and CYP3A4 metabolic assessment

We next evaluated drug transporters and metabolic capacity in the porcine MPS chip. Two efflux transporters, BCRP and P-gp, are highly expressed in intestinal tissue in vivo. Live cell fluorescence imaging was conducted on the organ chips with known substrates and inhibitors of each transporter in order to determine if those transporters were active at the apical boundary of the epithelium. The fluorescent BCRP substrate, BODIPY-prazosin, did not appreciably accumulate in the top channel epithelium, as shown in the view from above in Fig. 8A. However, when BODIPY-prazosin was cotreated with the BCRP inhibitor, chrysin, intestine chips had a much larger fluorescent signature (Fig. 8B), which suggested that the BCRP drug transporter was active in the epithelium cultures.

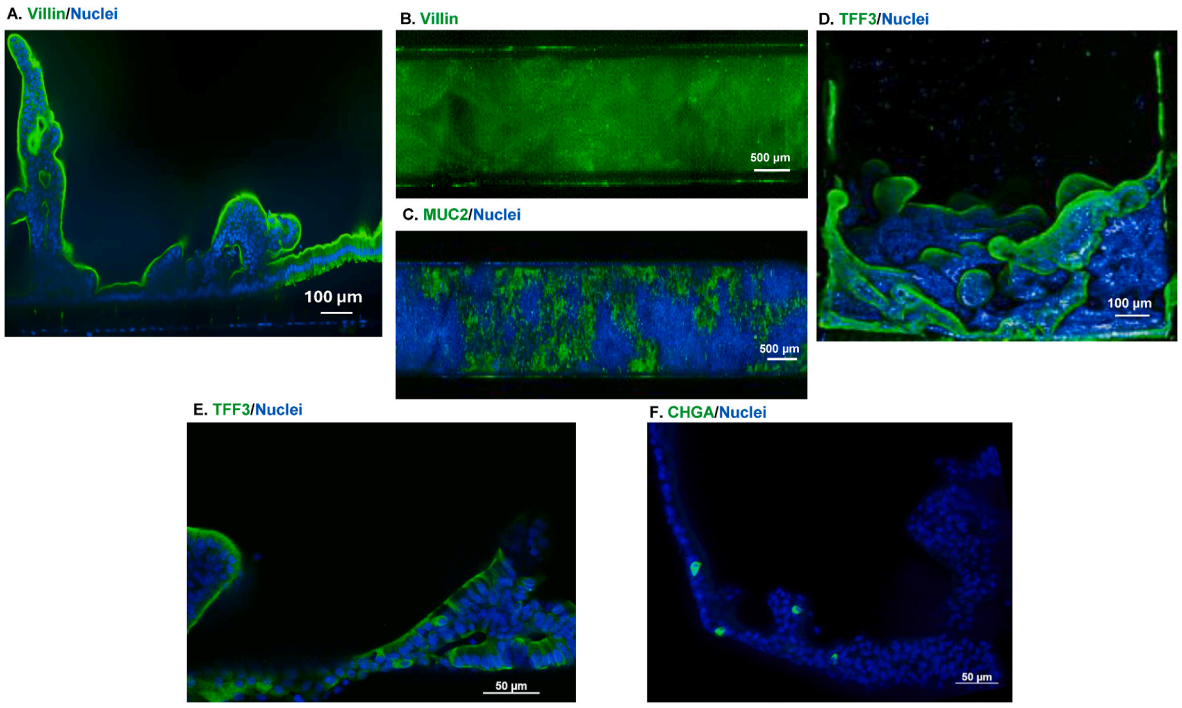

Fig. 6. Confocal immunofluorescent microscopy of Day 10 porcine jejunum chips. Representative images show the presence of the brush border component, villin (panels A and B), as expressed by enterocytes. Panel A is a cross-section showing villin (green) at the apical boundary of the epithelium. Panel B is a view from above demonstrating the appearance of villin throughout the length of the chip. Evidence of goblet cells is shown by MUC2 and TFF3 detection in panels C–E. MUC2 staining (green) is seen in Panel C in a view from above. TFF3 is observed in the cross-sectional slices in Panels D and E. The higher resolution image in Panel D shows apical layering of TFF3 as well as a sparse population of goblet cells with intracellular localization of TFF3. Panel E is a lower resolution 477 μm z-stack max projection image of the entire chip in cross-section, demonstrating the extensive presence of TFF3 throughout the apical surface of the epithelium. In Panel F, enteroendocrine cells are shown in cross section by CHGA-staining (green). Blue indicates Hoechst-stained nuclei.

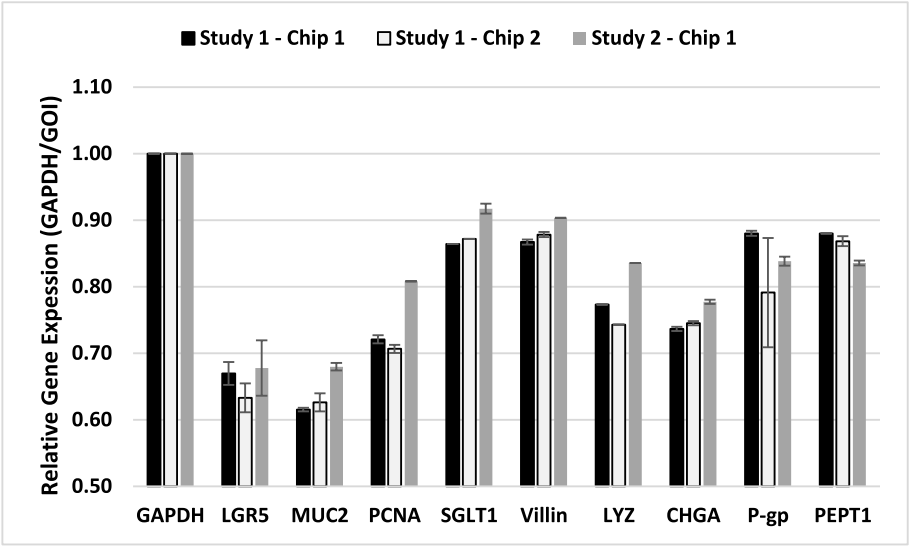

Fig. 7. Relative gene expression in porcine jejunum chips. Genes normally present in jejunum were analyzed in organ chip cultures by RT-PCR from two separate studies. Duplicate chips from Study 1 (Day 10, black and light grey bars) and a chip from Study 2 (Day 11, dark grey bar) were evaluated in order to assess overall expression relative to GAPDH, as well as intra- and inter-study variability. Results were expressed by calculating the ratio of the GAPDH Ct/gene of interest (GOI) Ct and shown as the mean ± standard deviation (n = 3).

P-gp was assessed in an experimental design similar to BCRP. Rhodamine 123, a substrate of P-gp, was used as a general measure of transporter activity by live cell fluorescence uptake in the jejunum MPS. Fig. 8C demonstrated minimal accumulation of rhodamine 123 in jejunum chip cultures, consistent with expectations. Cotreatment with the P-gp inhibitor, LSN335984 (Fig. 8D), resulted in greater accumulation of rhodamine 123 than the uninhibited treatment group, which indicated that P-gp was a functional transporter in the jejunum chips. Additional evidence for functional P-gp was underscored in studies designed to measure the flux of substrate from the top to the bottom channel. For these studies, vincristine served as the prototypical P-gp substrate and was quantified by LC/MS-MS methods in both the top

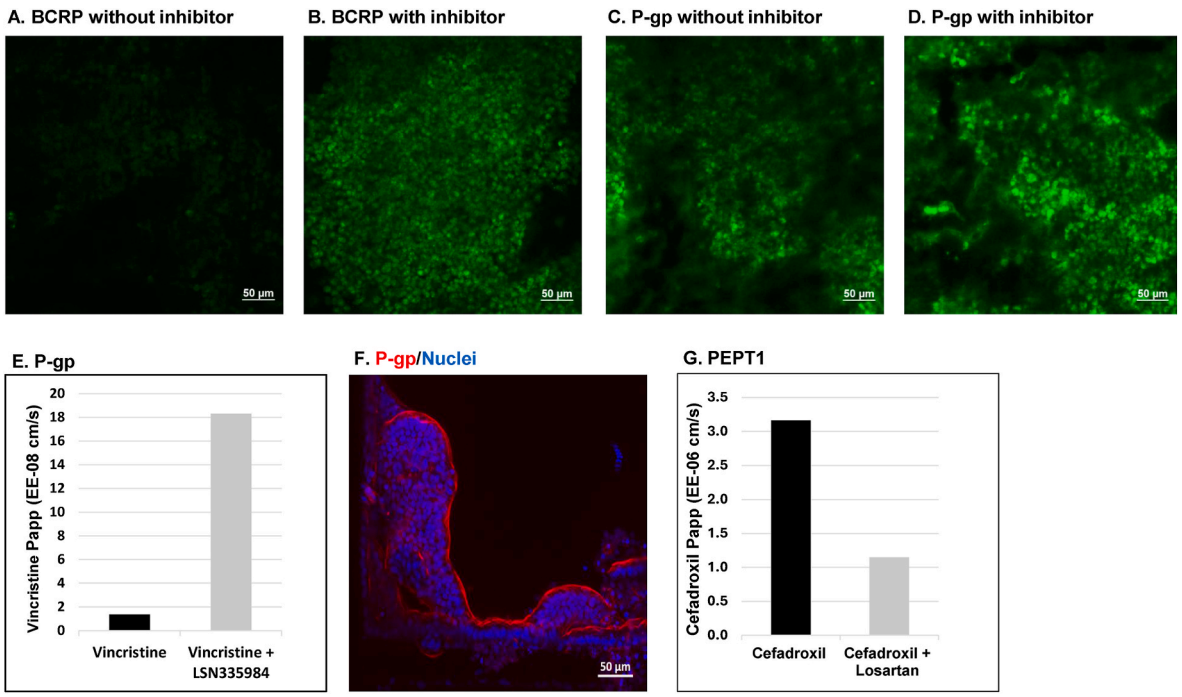

Fig. 8. Drug transporter function was assessed for the efflux transporters, BCRP and P-gp, and the uptake transporter, PEPT1. For BCRP, imaging was done on jejunum chips in the presence of the fluorescent substrate, BODIPY-prazosin (panel A), and as a cotreatment with the BCRP inhibitor, chrysin (panel B). For P-gp, imaging was done on jejunum chips in the presence of the fluorescent substrate, rhodamine 123 (panel C), and as a cotreatment with the P-gp inhibitor, LSN335984 (panel D). P-gp efflux transporter function was measured by quantifying the amount of vincristine, a P-gp substrate, or vincristine cotreated with the P-gp inhibitor, LSN335984 (panel E), present in the top and bottom channel outlets of intestine chips following a 3 h of treatment. Panel F is a representative cross-sectional confocal micrograph showing IF staining of P-gp on the apical surface of the epithelium. In Panel G, PEPT1 was evaluated by quantifying the amount of the substrate, cefadroxil, present in top and bottom channel outlets of chips when treated alone or in combination with the PEPT1 inhibitor, losartan, following a 3 h treatment. The accumulation of vincristine and cefadroxil were measured using LC/MS methods and expressed as the averaged P_{app} values (n = 2).

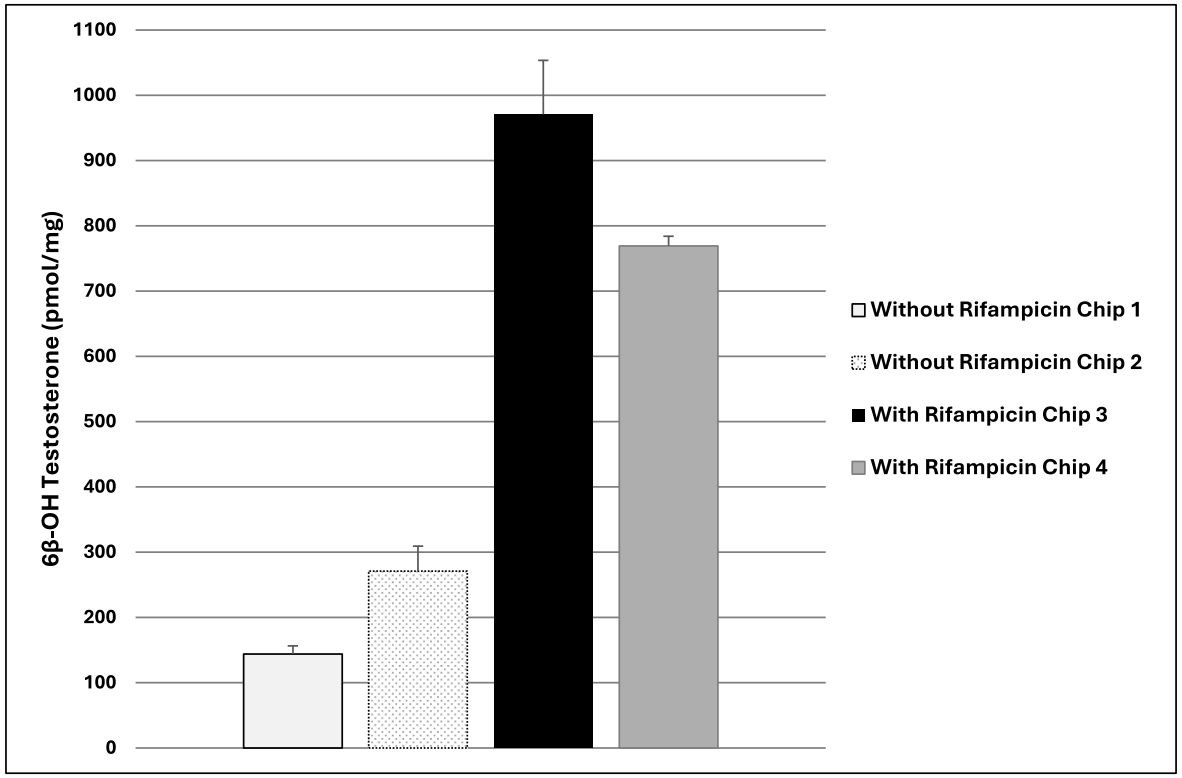

Fig. 9. CYP3A metabolic activity was demonstrated in jejunum chips by measuring CYP3A-mediated formation of 6β-hydroxy testosterone. Chips were pre-treated with 20 µM rifampicin or vehicle for 48 h, followed by incubation with 50 µM testosterone with or without rifampicin. 6β-hydroxy testosterone was measured after 24 h of treatment with testosterone and quantified using LC/MS-MS methods (n = 3).

and bottom channel outlet reservoirs. Fig. 8E show the results of the vincristine P-gp transporter study. Vincristine treatment alone at 3 h was largely excluded from the bottom channel but in the presence of the inhibitor, LSN335984, the apparent permeability increased nearly 10-fold, further supporting that the efflux transporter was functional. The IF image shown in Fig. 8F lends additional evidence for a luminal presence of P-gp (shown in red) on the epithelium cultures.

In addition to efflux transporters, BCRP and P-gp, the uptake transporter, PEPT1, was also assessed. The flux of the PEPT1 substrate, cefadroxil, was measured from the luminal to abluminal side of intestine chips, following a 3 h treatment in the absence or presence of the losartan, a PEPT1 inhibitor. In Fig. 8G, the P_{app} value for cefadroxil was greater in the cefadroxil treatment alone compared to cotreatment with losartan. This result is consistent with a functioning PEPT1 transporter.

CYP3A-mediated metabolism was also investigated in the porcine jejunum chip cultures. The formation of the 6β-hydroxytestosterone metabolite from testosterone is a result of CYP3A metabolism and was used as an indicator of enzyme activity. Chips were pretreated with DMSO (0.1 %) or 20 μM rifampicin for 48 h followed by 24 h cotreatment with 50 μM testosterone in order to determine if CYP3A was present and if it was inducible. The results demonstrated measurable levels of 6β-hydroxytestosterone present in the vehicle control group (without rifampicin pretreatment) which showed a baseline level of CYP3A activity in the jejunum chip cultures (Fig. 9). Pretreatment with rifampicin resulted in 4.2-fold greater metabolite formation of 6β-hydroxytestosterone, consistent with an inducible CYP3A response.

3.6. Permeability assessment in the absence or presence of a permeation enhancer

Studies were conducted to determine the response of the jejunum MPS to permeability enhancer treatment. C_{10}, a well-established permeation enhancement agent, was used to increase barrier permeability as determined by quantifying the passive permeability markers, 3 kDa dextran and Lucifer Yellow, in the epithelial and endothelial compartments of the organ chips. A 90 min treatment of the jejunum MPS was performed using a standard flow rate of 30 μL/h. In order to generate adequate volumes of media in the outlet reservoirs to assay early timepoints (2 and 4 h posttreatment), the flow rate was increased to 50 μL/h before adjusting back to 30 μL/h for the 24 and 48 h sample collections. The results shown in Fig. 10A and B demonstrated that C_{10} treatment caused a concentration-dependent increase in permeability for both dextran and Lucifer Yellow. The increased permeability was particularly prominent at the 2 and 4 h posttreatment timepoints. The maximum change from control chip permeability measurements was 3.5- and 2.3-fold increase for dextran and Lucifer Yellow, respectively, at 4 h. The changes in apparent permeability were significantly different ($p < 0.05$) compared to control groups for dextran at 4 h and for Lucifer Yellow at 2 and 4 h timepoints. Further, the progression at 24 and 48 h posttreatment was most noteworthy. The results indicated that the barrier tightness in the 10 and 25 mM dose groups was restored as evidenced by dextran and Lucifer Yellow permeability, and the P_{app} values for all accompanying LDH data (Fig. 10C) for the 24 and 48 h timepoints suggest C_{10} treatment did not adversely affect cell viability.

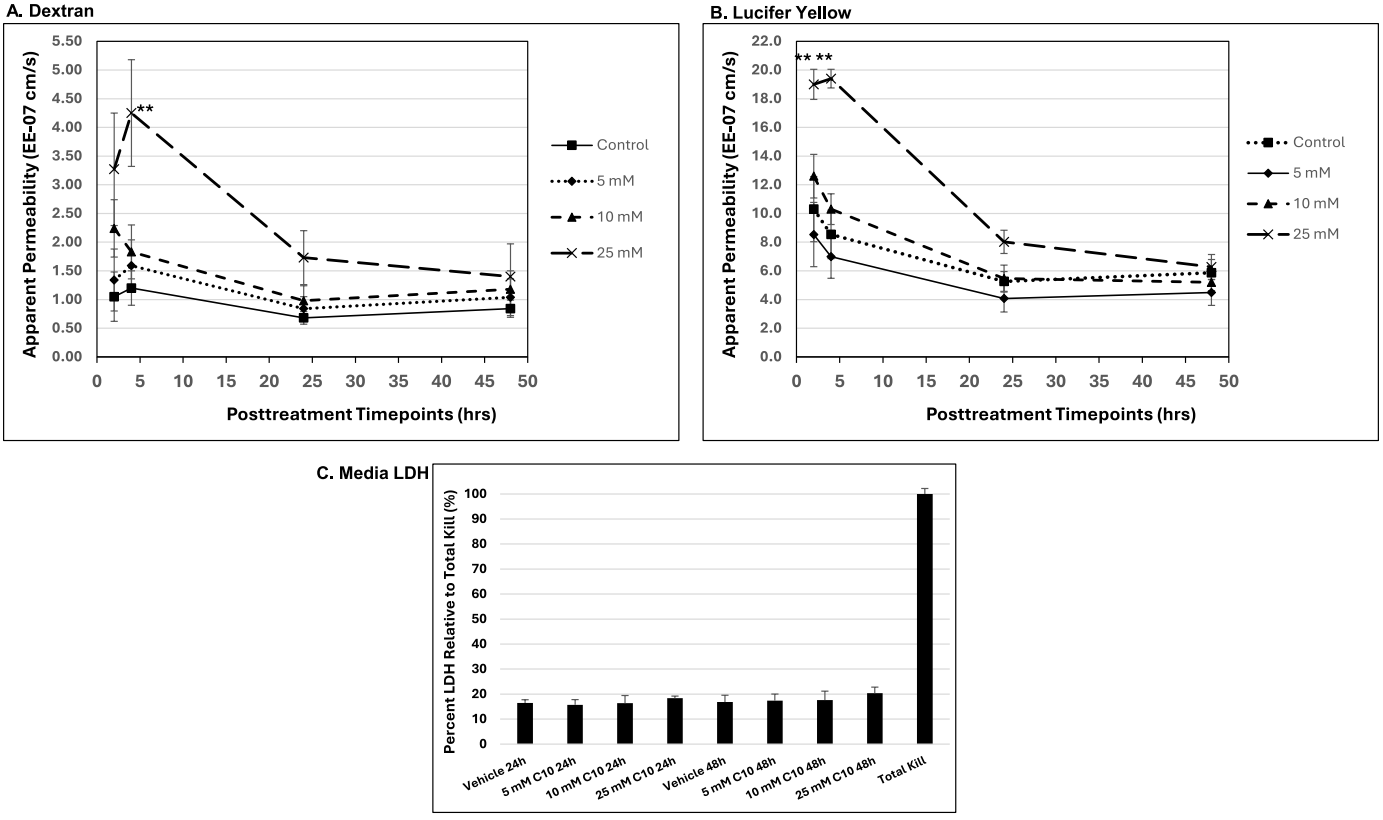

Fig. 10. Effects of sodium caprate on jejunum chip permeability using 3 kDa Cascade Blue Dextran (A) and 0.4 kDa Lucifer Yellow (B) fluorescent markers. Permeability enhancement studies using various concentrations of sodium caprate (5, 10 and 25 mM) added to the top channel were initiated on day 8 or day 9 jejunum chips. Chips were treated for 90 min with sodium caprate or vehicle, and in the presence of 3 kDa dextran and Lucifer Yellow. Following the treatment, the dose solutions were removed from the top channel inlet reservoir and replaced with culture media supplemented with dextran and Lucifer Yellow. Samples were collected from top and bottom channel outlets at 2, 4, 24 and 48 h posttreatment to determine the apparent permeability values of dextran (panel A) and Lucifer Yellow (panel B). Media was also evaluated for LDH release at 24 and 48 h posttreatment (panel C). An ANOVA was performed on the averaged P_{app} values ± standard error; n = 4 per group. **$P < 0.05$ compared to untreated controls.

4. Discussion

Our aim was to establish a porcine jejunum MPS organ chip, which has not previously been reported. The jejunum chip was characterized for cellular composition and functions normally associated with jejunum tissue. In addition, we expanded our characterization to include aspects within the area of absorption, distribution, metabolism, elimination and toxicology (ADMET). At present, the use of crypt-derived organoids for intestinal organ chip models is limited [24]. The majority of the gut chip work reported utilize Caco-2 cells. While the addition of flow and stretch to Caco-2 cells grown in a microfluidic environment improved the intestinal characteristics to more closely resemble in vivo tissue compared to a static flow in vitro system [14], it was demonstrated that intestinal material from organoids cultured in an MPS demonstrated a superior transcriptomic gene profile comparison to in vivo tissue than the Caco gut chip, as well as better functionality [15]. Thus, the pairing of intestinal organoids and microengineering technology has afforded an opportunity to develop revolutionary in vitro models, greatly improving IVIVE and making the drug development process more efficient.

Intestinal organoids undergo self-organization and renewal, as well as to create function and an architecture resembling the tissue from which they are derived. Furthermore, they are able to generate the main cell types that comprise the mucosal epithelial layer in the gut. We adapted the seeding and growth protocol for porcine jejunum organoids that had been recommended for human duodenal organoids ([25]). The cell growth of the top channel epithelium in the porcine jejunum MPS chips paralleled the morphogenesis observed in the adult human intestine chip cultures, culminating in a demarcated, cuboidal epithelial shape, with prominent vertical growth [23]. The morphology of the epithelium demonstrated architecture reminiscent of villi-like structures. The jejunum chip MPS cultures also included an extensive formation of F-actin and the tight junctions, ZO-1 and E-cadherin. HIMECs seeded into the bottom channels of chips quickly formed monolayers after media flow was initiated (<12 h). Based on previously published work with this MPS format [15,23], it was well-established that an organ chip model would most effectively recapitulate intestinal tissue in a co-cultured environment, having an epithelial-endothelial cell interface. Interactions between cells on either side of porous EM-coated membrane provided a conduit between the epithelium and endothelium. The 50 μm thick PDMS chips, with 7 μm pores spaced 40 μm apart, did not pose a significant permeability barrier. The P_{app} of 3 kDa dextran was >43-fold higher in chips with HIMECs alone than a co-cultured jejunum MPS (unpublished data). Indeed, the intestine chips established a tight barrier ($P_{app} < 2.5 \times 10^{-7}$ cm/s) from day 7 on, as demonstrated with 3 kDa dextran permeability marker. The lower molecular weight marker, Lucifer Yellow (400 Da), also confirmed barrier tightness but had higher P_{app} values that stabilized at approximately 4×10^{-7} cm/s, compared to approximately 1×10^{-7} cm/s for dextran, suggesting a size-dependent paracellular permeability distinction between the two markers. The Lucifer Yellow P_{app} values were similar to those reported previously in human duodenal chips using a co-culture format [15].

In vivo, the intestinal epithelium is in a constant state of renewal as a result of the highly proliferative stem cells residing in the crypts at the base of the villi. An intact crypt region is fundamental to any in vitro model intended to recapitulate intestinal tissue. We determined the porcine jejunum chips had a distinct region undergoing active cell proliferation which was compartmentalized to the basolateral boundary. The localization was limited to the cells comprising the area at the base of the villi-like projections and did not extend above the lowest levels of Z-axis epithelial growth, consistent with the human intestine organoid MPS [15]. There was a noteworthy time-dependence of cell proliferation which showed a progression toward fewer cells stained for Ki-67 with increasing days in culture. Early timepoints that had robust proliferation, coincided with use of media intended to establish pre-differentiated cell growth. The Ki-67-positively stained cells began to diminish in numbers after media was changed over to enhance differentiation of the epithelium. The decline in numbers of proliferating cells overlapped with morphological changes around Day 11 or 12, which were characterized by a decrease in cuboidal epithelial structure. The Ki-67 and EdU results, indicating the presence of crypts, were also confirmed by gene expression analysis. Lgr5, produced in cycling crypt-based columnar cells, and lysozyme, a marker of Paneth cells, were both detected by RT-PCR in relative expression patterns consistent with their anticipated populations in the jejunum chips [1,26]. The confirmed presence of an active crypt-like region provided greater evidence that the organ chip model contained important aspects of intact jejunum.

In contrast to the temporal reduction of proliferation activity, citrulline levels increased over time suggesting a greater abundance of enterocytes and further differentiation of the jejunum MPS cultures. An inflection point occurred around Day 8 of culture growth when the combination of co-cultured epithelium and HIMECs, along with dynamic stretch and media flow, triggered a marked increase in epithelial differentiation. Morphological changes observed via phase-contrast microscopy directly coincided with the generation of citrulline. This altered morphology had the appearance of a 'beehive' in cross section, and served as a useful indicator of when the jejunum chips were suitable to conduct studies. Villin protein was particularly notable for its localization to the apical surface of the epithelium as well as the extent to which it covered the top channel. The position and area of coverage were consistent with the appearance of villin in other gut chip models as well as in vivo.

Additional evidence that the epithelium had undergone extensive differentiation toward a preponderance of enterocyte cells was provided by the relative gene expression profiles of SGLT1 and villin. These two enterocyte markers had the largest relative gene expression values of various genes assayed, consistent with the in vivo expression profile of porcine ileum [27] and human colon [28]. Moreover, goblet cells and enteroendocrine cells were also detected in the jejunum MPS cultures, further indicating the development of a differentiated epithelium. Especially noteworthy was the generation of a mucosal layer suggesting a functional population of goblet cells. IF staining of MUC2 and TFF3 showed a mucous layer forming predominantly on the apical surface of the epithelium. The gene expression profile also confirmed the presence of MUC2. Demonstration of enteroendocrine cells was denoted by CHGA gene expression and IF staining. The relatively few numbers of cells staining positively for CHGA was in parallel to the anticipated distribution of enteroendocrine cells along the jejunum epithelium. The staining characteristics of CHGA was cytoplasmic in nature, limited to isolated cells in the jejunum MPS chip, and was in sharp contrast to the staining pattern of enterocyte and goblet cell markers. The staining patterns of the various cell types were similar to previous findings in human intestine chips [15,29].

We also evaluated the in vitro model for function typically found in the small intestine. There are numerous drug transporters present along the luminal and basolateral boundaries. In human tissue, PEPT1 is expressed to the largest extent, with BCRP and P-gp also among the more highly expressed drug transporters [30]. The jejunum organ chips demonstrated BCRP and P-gp transporter function at the apical boundary, and vectoral transport by PEPT1 and P-gp from the top channel into the bottom channel was also confirmed. Further, gene expression profiles supported evidence of robust PEPT1 and P-gp drug transporter presence in the epithelium, consistent with the functional results. Taken together, evidence of functional drug transporters in the jejunum chips further support the potential use of this model for mechanistic studies.

Another ADME property that was characterized in the organ chips was metabolic activity. While the list of metabolic enzymes is extensive, CYP3A4 is the most important among the P450 enzymes. CYP3A is the porcine equivalent of human CYP3A4. The assessment of metabolic capacity of the chips successfully showed an endogenous activity that converted testosterone to the 6β-hydroxytestosterone metabolite, similar to the metabolism in vivo in porcine jejunum [31]. CYP3A

activity in jejunum chips was also inducible, consistent with expectations, and a response qualitatively similar to human duodenum chips [23]. The extent of 6β-hydroxytestosterone metabolite formed was substantially less in the porcine jejunum chips compared to the human duodenum chips which may be attributed to species differences. Nevertheless, this additional level of characterization of the porcine jejunum chips further supports it as an attractive in vitro intestinal model.

While there is a growing list of potential conditions that gut-on-a-chip MPS formats are being directed towards, such as assessing microbial interplay with the epithelium [32], measuring oral prodrug conversion [33] or modelling chronic intestinal disorders [34] to cite only a few, the application of those established in vitro models is presently outside the scope of the jejunum MPS we report. Nevertheless, after confirming the jejunum MPS recapitulated many aspects of in vivo jejunum, we sought to determine whether an important function of this in vitro model could replicate the in vivo response. The potential utility of the jejunum MPS model was evaluated through permeation enhancement studies. With the increased development of large molecule pharmaceuticals, the challenge to circumvent barriers in the gastrointestinal (GI) tract is highlighted, and better in vitro models are needed to assist preclinical decisions. The delivery of large molecules across the intestinal epithelium is problematic due to low bioavailability, which can be improved upon by permeability enhancers. Existing permeation enhancers, sodium N-(82-hydroxybenzoyl amino) caprylate (SNAC) and sodium caprylate (C_8), are used in oral formulations of approved pharmaceuticals [35,36]. Sodium caprate (C_{10}) is another commonly used permeation enhancer which is an approved component of Doktacillin®, an ampicillin suppository [37]. C_{10} has also been tested in clinical trials in oral dosage forms for a range of molecules with limited permeability [38]. Intestinal models that can better predict large molecule permeability hold promise for identifying drug candidates that are more likely to achieve clinical success. Some of those models include ex vivo intestinal tissue used in conjunction with an Ussing chamber, in vivo methods using oral gavage and in situ methods with intra-intestinal instillation of intact tissue [39–42]. Caco-2 cells have been the most extensively used in vitro model for permeation enhancement studies thus far [43,44].

Previous work on Caco-2 cells in a Transwell format evaluated C_{10} for a variety of endpoints including cytotoxicity, mechanism of action, as well as paracellular flux measurements [43,44]. In the current study, our work in the jejunum MPS focused on the paracellular movement of marker compounds after treatment with varying concentrations of C_{10}, followed by a 48 h recovery phase. The duration of C_{10} treatment in our studies was 90 min which approximated Caco-2 exposure times. There was a concentration-dependent increase in permeability in the jejunum chips which was accompanied by a relatively steep cytotoxic dose-response. The morphological observation of cultures incubated with 50 mM C_{10} showed that the epithelial layer of cells in the top channel had become detached and was largely absent, while the 25 mM C_{10} concentration had an intact monolayer. A similarly steep cytotoxic concentration response was observed in Caco-2 cells with C_{10} at 10 mM causing no significant increase in LDH whereas 20 mM showed complete lethality [44]. The jejunum MPS showed maximum increase in permeability of both large and small molecular weight markers at 2 and/or 4 h posttreatment. This finding paralleled the Caco-2 results which demonstrated maximum increase also at 2 h posttreatment [43]. For the jejunum MPS chips, the 25 mM C_{10} concentration resulted in significant changes in P_{app} values. The 5 and 10 mM C_{10} concentrations also affected permeability but did not achieve statistical significance. By 24 h posttreatment, the jejunum MPS treated with 25 mM C_{10} were not significantly different from control chips, and by 48 h the P_{app} values were nearly identical to control values. These data demonstrated that full recovery from barrier opening occurred in the porcine jejunum MPS model.

The barrier opening and recovery from permeation enhancement we observed is similar to various intestinal animal models as well as in humans [21,42,45]. Epithelial damage and perturbation of the tight junctions following exposure to permeation enhancers, leading to an increase of paracellular movement, has been well established [21,22,42,43]. In a similar manner, the disruption C_{10} caused to the epithelium in the jejunum MPS resulted in an altered morphological appearance suggesting the villi-like structures had been compromised, leading to a subsequent increase in paracellular permeability. This event is reminiscent of descriptions in various intestinal models. The mechanism by which the barrier opening occurred, such as that explored by Twarog et al. [44] in Caco-2 cells cultures exposed to C_{10} or SNAC, was beyond the focus of this project. Most significantly though, and comparable to other models, is the recovery that the jejunum MPS chips undergo.

Barrier opening following C_{10} treatment was also observed in porcine jejunum organoid cultures grown in a Transwell system, as determined by increased TEER values [22]. However, the Transwell porcine organoid monolayers failed to recover after exposure to the C_{10} (data not shown) in contrast to the porcine jejunum MPS. This result further highlights the importance of a differentiated state present in the jejunum MPS versus traditional static culture models. Although previously noted that Caco-2 cells grown in an MPS format developed characteristics that are more closely aligned with normal epithelial growth [46], the derivation of this cell line from colon adenocarcinoma cells represent a stark contrast to jejunum organoids from which the porcine jejunum MPS originated.

We recognize the jejunum MPS has certain technical challenges that a cell line-based in vitro model may not have. Isolating organoids from porcine jejunum is not without a level of complexity and precision, as is the growth of organoid cultures in Matrigel domes. Further, uniformity in the dissociation of organoid spheres into single cells and fragments lends greater predictability in the growth of organ chips from one isolation to the next. Thus, the complexity of this in vitro model is commensurate with the labor-intensity required to culture optimal organ chips. From a pharmaceutical research perspective, the jejunum MPS we describe is better aligned with a low throughput stage in the drug development process as opposed to early discovery involving high numbers of test compounds. Nevertheless, its use as a mechanistic tool is highly anticipated. The microfluidic device we employ allows for ease of use and enables the cellular architecture resembling villi to develop de novo in the absence of an artificial scaffold that some biofabricated platforms utilize (for review see Ref. [47]). Overall, given that the porcine jejunum MPS supports the 3Rs, requires fewer resources and less effort to establish than most in vivo, ex vivo or in situ models, we believe it would serve as a suitable surrogate for conducting intestinal mechanistic studies.

5. Conclusions

An organoid-based pig jejunum MPS was developed using the Emulate platform. The organ chip was characterized for the presence of numerous cellular and biochemical markers, gene expression of villi and crypt cells, as well as various drug transporters and metabolic activity associated with jejunum. Further, this jejunum chip model responded to permeability enhancement treatment in a manner consistent with in vivo tissue by reversibly opening and retightening following treatment with C_{10}. Preclinical testing applications using this model offer alternatives to existing in vitro intestinal models. This work represents a next step in the progression of novel models utilizing organoid research and the potential advancement for more effective drug development.

Declaration of competing interest

The authors declare that they have no known competing financial interests or personal relationships that could have appeared to influence the work reported in this paper.

Acknowledgements

All funding for this research was provided by Eli Lilly and Company.

Appendix A. Supplementary data

Supplementary data to this article can be found online at https://doi.org/10.1016/j.bbrep.2025.102036.

References

[1] N. Barker, J.H. van Es, J. Kuipers, P. Kujala, M. van den Born, M. Cozijnsen, A. Haegebarth, J. Korving, H. Begthel, P.J. Peters, H. Clevers, Identification of stem cells in small intestine and colon by marker gene Lgr5, Nature 449 (7165) (2007 Oct 25) 1003–1007, https://doi.org/10.1038/nature06196. Epub 2007 Oct 14. PMID: 17934449.

[2] T. Sato, R.G. Vries, H.J. Snippert, M. van de Wetering, N. Barker, D.E. Stange, J. H. van Es, A. Abo, P. Kujala, P.J. Peters, H. Clevers, Single Lgr5 stem cells build crypt-villus structures in vitro without a mesenchymal niche, Nature 459 (7244) (2009 May 14) 262–265, https://doi.org/10.1038/nature07935. Epub 2009 Mar 29. PMID: 19329995.

[3] L. Chandra, D.C. Borcherding, D. Kingsbury, T. Atherly, Y.M. Ambrosini, A. Bourgois-Mochel, W. Yuan, M. Kimber, Y. Qi, Q. Wang, M. Wannemuehler, N. M. Ellinwood, E. Snella, M. Martin, M. Skala, D. Meyerholz, M. Estes, M. E. Fernandez-Zapico, A.E. Jergens, J.P. Mochel, K. Allenspach, Derivation of adult canine intestinal organoids for translational research in gastroenterology, BMC Biol. 17 (1) (2019 Apr 11) 33, https://doi.org/10.1186/s12915-019-0652-6. PMID: 30975131; PMCID: PMC6460554.

[4] R.H. Powell, M.S. Behnke, WRN conditioned media is sufficient for *in vitro* propagation of intestinal organoids from large farm and small companion animals, Biol Open 6 (5) (2017 May 15) 698–705, https://doi.org/10.1242/bio.021717. PMID: 28347989; PMCID: PMC5450310.

[5] H. Derricott, L. Luu, W.Y. Fong, C.S. Hartley, L.J. Johnston, S.D. Armstrong, N. Randle, C.A. Duckworth, B.J. Campbell, J.M. Wastling, J.L. Coombes, Developing a 3D intestinal epithelium model for livestock species, Cell Tissue Res. 375 (2) (2019 Feb) 409–424, https://doi.org/10.1007/s00441-018-2924-9. Epub 2018 Sep 26. PMID: 30259138; PMCID: PMC6373265.

[6] L.M. Gonzalez, I. Williamson, J.A. Piedrahita, A.T. Blikslager, S.T. Magness, Cell lineage identification and stem cell culture in a porcine model for the study of intestinal epithelial regeneration, PLoS One 8 (6) (2013 Jun 28) e66465, https://doi.org/10.1371/journal.pone.0066465. PMID: 23840480; PMCID: PMC3696067.

[7] H.A. Khalil, N.Y. Lei, G. Brinkley, A. Scott, J. Wang, U.K. Kar, Z.B. Jabaji, M. Lewis, M.G. Martín, J.C. Dunn, M.G. Stelzner, A novel culture system for adult porcine intestinal crypts, Cell Tissue Res. 365 (1) (2016 Jul) 123–134, https://doi.org/10.1007/s00441-016-2367-0. Epub 2016 Mar 1. PMID: 26928041; PMCID: PMC4919165.

[8] H. Li, Y. Wang, M. Zhang, H. Wang, A. Cui, J. Zhao, W. Ji, Y.G. Chen, Establishment of porcine and monkey colonic organoids for drug toxicity study, Cell Regen. 10 (1) (2021 Oct 2) 32, https://doi.org/10.1186/s13619-021-00094-4. PMID: 34599392; PMCID: PMC8486901.

[9] C. Moon, K.L. VanDussen, H. Miyoshi, T.S. Stappenbeck, Development of a primary mouse intestinal epithelial cell monolayer culture system to evaluate factors that modulate IgA transcytosis, Mucosal Immunol. 7 (4) (2014 Jul) 818–828, https://doi.org/10.1038/mi.2013.98. Epub 2013 Nov 13. PMID: 24220295; PMCID: PMC4019725.

[10] Y. Wang, M. DiSalvo, D.B. Gunasekara, J. Dutton, A. Proctor, M.S. Lebhar, I. A. Williamson, J. Speer, R.L. Howard, N.M. Smiddy, S.J. Bultman, C.E. Sims, S. T. Magness, N.L. Allbritton, Self-renewing monolayer of primary colonic or rectal epithelial cells, Cell. Mol. Gastroenterol. Hepatol. 4 (1) (2017 Mar 6) 165–182.e7, https://doi.org/10.1016/j.jcmgh.2017.02.011. PMID: 29204504; PMCID: PMC5710741.

[11] E.H. Fernando, M. Dicay, M. Stahl, M.H. Gordon, A. Vegso, C. Baggio, L. Alston, F. Lopes, K. Baker, S. Hirota, D.M. McKay, B. Vallance, W.K. MacNaughton, A simple, cost-effective method for generating murine colonic 3D enteroids and 2D monolayers for studies of primary epithelial cell function, Am. J. Physiol. Gastrointest. Liver Physiol. 313 (5) (2017 Nov 1) G467–G475, https://doi.org/10.1152/ajpgi.00152.2017. Epub 2017 Jul 27. PMID: 28751424.

[12] B. van der Hee, L.M.P. Loonen, N. Taverne, J.J. Taverne-Thiele, H. Smidt, J. M. Wells, Optimized procedures for generating an enhanced, near physiological 2D culture system from porcine intestinal organoids, Stem Cell Res. 28 (2018 Apr) 165–171, https://doi.org/10.1016/j.scr.2018.02.013. Epub 2018 Feb 20. PMID: 29499500.

[13] M.B. Esch, J.H. Sung, J. Yang, C. Yu, J. Yu, J.C. March, M.L. Shuler, On chip porous polymer membranes for integration of gastrointestinal tract epithelium with microfluidic 'body-on-a-chip' devices, Biomed. Microdevices 14 (2012 Jul) 895–906.

[14] H.J. Kim, D.E. Ingber, Gut-on-a-Chip microenvironment induces human intestinal cells to undergo villus differentiation, Integr. Biol. 5 (9) (2013 Sep) 1130–1140, https://doi.org/10.1039/c3ib40126j. PMID: 23817533.

[15] M. Kasendra, A. Tovaglieri, A. Sontheimer-Phelps, S. Jalili-Firoozinezhad, A. Bein, A. Chalkiadaki, W. Scholl, C. Zhang, H. Rickner, C.A. Richmond, H. Li, D. T. Breault, D.E. Ingber, Development of a primary human Small Intestine-on-a-Chip using biopsy-derived organoids, Sci. Rep. 8 (1) (2018 Feb 13) 2871, https://doi.org/10.1038/s41598-018-21201-7. PMID: 29440725; PMCID: PMC5811607.

[16] G. Bode, P. Clausing, F. Gervais, J. Loegsted, J. Luft, V. Nogues, J. Sims, Steering Group of the RETHINK Project, The utility of the minipig as an animal model in regulatory toxicology, J. Pharmacol. Toxicol. Methods 62 (3) (2010 Nov-Dec) 196–220, https://doi.org/10.1016/j.vascn.2010.05.009. Epub 2010 May 31. PMID: 20685310.

[17] D.T. Schomberg, A. Tellez, J.J. Meudt, D.A. Brady, K.N. Dillon, F.K. Arowolo, J. Wicks, S.D. Rousselle, D. Shanmuganayagam, Miniature swine for preclinical modeling of complexities of human disease for translational scientific discovery and accelerated development of therapies and medical devices, Toxicol. Pathol. 44 (3) (2016 Apr) 299–314, https://doi.org/10.1177/0192623315618292. Epub 2016 Feb 2. PMID: 26839324.

[18] H. Tang, M. Mayersohn, Porcine prediction of pharmacokinetic parameters in people: a pig in a poke? Drug Metab. Dispos. 46 (11) (2018 Nov) 1712–1724, https://doi.org/10.1124/dmd.118.083311. Epub 2018 Aug 31. PMID: 30171162.

[19] L.J. Henze, N.J. Koehl, J.P. O'Shea, E.S. Kostewicz, R. Holm, B.T. Griffin, The pig as a preclinical model for predicting oral bioavailability and in vivo performance of pharmaceutical oral dosage forms: a PEARRL review, J. Pharm. Pharmacol. 71 (4) (2019 Apr) 581–602, https://doi.org/10.1111/jphp.12912. Epub 2018 Apr 10. PMID: 29635685.

[20] S. Rahman, M. Ghiboub, J.M. Donkers, E. van de Steeg, E.A.F. van Tol, T.B. M. Hakvoort, W.J. de Jonge, The progress of intestinal epithelial models from cell lines to gut-on-chip, Int. J. Mol. Sci. 22 (24) (2021 Dec 15) 13472, https://doi.org/10.3390/ijms222413472. PMID: 34948271; PMCID: PMC8709104.

[21] F. McCartney, J.P. Gleeson, D.J. Brayden, Safety concerns over the use of intestinal permeation enhancers: a mini-review, Tissue Barriers 4 (2) (2016 Apr 12) e1176822, https://doi.org/10.1080/21688370.2016.1176822. PMID: 27358756; PMCID: PMC4910835.

[22] H. Tran, E. Aihara, F.A. Mohammed, H. Qu, A. Riley, Y. Su, X. Lai, S. Huang, A. Aburub, J.J.H. Chen, O.H. Vitale, Y. Lao, S. Estwick, Z. Qi, M.E.H. ElSayed, *In vivo* mechanism of action of sodium caprate for improving the intestinal absorption of a GLP1/GIP coagonist peptide, Mol. Pharm. 20 (2) (2023 Feb 6) 929–941, https://doi.org/10.1021/acs.molpharmaceut.2c00443. Epub 2023 Jan 2. PMID: 36592951.

[23] M. Kasendra, R. Luc, J. Yin, D.V. Manatakis, G. Kulkarni, C. Lucchesi, J. Sliz, A. Apostolou, L. Sunuwar, J. Obrigewitch, K.J. Jang, G.A. Hamilton, M. Donowitz, K. Karalis, Duodenum Intestine-Chip for preclinical drug assessment in a human relevant model, Elife 9 (2020 Jan 14) e50135, https://doi.org/10.7554/eLife.50135. PMID: 31933478; PMCID: PMC6959988.

[24] K.P. Van Ness, F. Cesar, C.K. Yeung, J. Himmelfarb, E.J. Kelly, Microphysiological systems in absorption, distribution, metabolism, and elimination sciences, Clin. Transl. Sci. 15 (1) (2022 Jan) 9–42, https://doi.org/10.1111/cts.13132. Epub 2021 Aug 26. PMID: 34378335; PMCID: PMC8742652.

[25] Emulate: Duodenum intestine-chip culture protocol. 2020 Jan 24; EP184 v1.0.

[26] D. Wang, K. Peregrina, E. Dhima, E.Y. Lin, J.M. Mariadason, L.H. Augenlicht, Paneth cell marker expression in intestinal villi and colon crypts characterizes dietary induced risk for mouse sporadic intestinal cancer, Proc. Natl. Acad. Sci. U. S. A. 108 (25) (2011 Jun 21) 10272–10277, https://doi.org/10.1073/pnas.1017668108. Epub 2011 Jun 7. PMID: 21652773; PMCID: PMC3121808.

[27] X. Ji, P. Lyu, R. Hu, W. Yao, H. Jiang, Generation of an enteric smooth muscle cell line from the pig ileum, J. Anim. Sci. 98 (4) (2020 Apr 1) skaa102, https://doi.org/10.1093/jas/skaa102. PMID: 32249920; PMCID: PMC7179811.

[28] P.C.M. Urbano, H.C.K. Angus, S. Gadeock, M. Schultz, R.A. Kemp, Assessment of source material for human intestinal organoid culture for research and clinical use, BMC Res. Notes 15 (1) (2022 Feb 10) 35, https://doi.org/10.1186/s13104-022-05925-4. PMID: 35144661; PMCID: PMC8830126.

[29] D.E. Levin, E.R. Barthel, A.L. Speer, F.G. Sala, X. Hou, Y. Torashima, T. C. Grikscheit, Human tissue-engineered small intestine forms from postnatal progenitor cells, J. Pediatr. Surg. 48 (1) (2013 Jan) 129–137, https://doi.org/10.1016/j.jpedsurg.2012.10.029. PMID: 23331805.

[30] M. Nishimura, S. Naito, Tissue-specific mRNA expression profiles of human ATP-binding cassette and solute carrier transporter superfamilies, Drug Metabol. Pharmacokinet. 20 (6) (2005 Dec) 452–477, https://doi.org/10.2133/dmpk.20.452. PMID: 16415531.

[31] H.A. Thörn, A. Lundahl, J.A. Schrickx, P.A. Dickinson, H. Lennernäs, Drug metabolism of CYP3A4, CYP2C9 and CYP2D6 substrates in pigs and humans, Eur. J. Pharm. Sci. 43 (3) (2011 Jun 14) 89–98, https://doi.org/10.1016/j.ejps.2011.03.008. Epub 2011 Apr 5. PMID: 21447389.

[32] H. Wang, X.Y. You, G.P. Zhao, Microbial volatile communication in human 3D intestinal organotypic models, Sci. Bull (Beijing). 68 (13) (2023 Jul 15) 1353–1358, https://doi.org/10.1016/j.scib.2023.05.030. Epub 2023 May 25. PMID: 37271716.

[33] A. Sharma, L. Jin, X. Wang, Y.T. Wang, D.M. Stresser, Developing an adult stem cell derived microphysiological intestinal system for predicting oral prodrug bioconversion and permeability in humans, Lab Chip 24 (2) (2024 Jan 17) 339–355, https://doi.org/10.1039/d3lc00843f. PMID: 38099395.

[34] A. Özkan, N.T. LoGrande, J.F. Feitor, G. Goyal, D.E. Ingber, Intestinal organ chips for disease modelling and personalized medicine, Nat. Rev. Gastroenterol. Hepatol. 21 (11) (2024 Nov) 751–773, https://doi.org/10.1038/s41575-024-00968-3. Epub 2024 Aug 27. PMID: 39192055.

[35] FDA. https://www.accessdata.fda.gov/drugsatfda_docs/label/2019/213051s000lbl.pdf, 2020. (Accessed 14 April 2020).

[36] S. Tuvia, D. Pelled, K. Marom, P. Salama, M. Levin-Arama, I. Karmeli, G.H. Idelson, I. Landau, R. Mamluk, A novel suspension formulation enhances intestinal absorption of macromolecules via transient and reversible transport mechanisms,

Pharm. Res. 31 (8) (2014 Aug) 2010–2021, https://doi.org/10.1007/s11095-014-1303-9. Epub 2014 Feb 21. PMID: 24558008; PMCID: PMC4153969.
[37] T. Lindmark, J.D. Söderholm, G. Olaison, G. Alván, G. Ocklind, P. Artursson, Mechanism of absorption enhancement in humans after rectal administration of ampicillin in suppositories containing sodium caprate, Pharm. Res. 14 (1997) 930–955, https://doi.org/10.1023/A:1012112219578.
[38] E. Walsh, B. Adamczyk, K.B. Chalasani, M. Maher, E.B. O'Toole, J. Fox, T. W. Leonard, D.J. Brayden, Oral delivery of macromolecules: rationale underpinning gastrointestinal permeation enhancement technology (GIPET®), Ther. Deliv. 2 (2011) 1595–1610, https://doi.org/10.4155/tde.11.132.
[39] J.P. Gleeson, J. Heade, S.M. Ryan, D.J. Brayden, Stability, toxicity and intestinal permeation enhancement of two food-derived antihypertensive tripeptides, Ile-Pro-Pro and Leu-Lys-Pro, Peptides 71 (2015 Sep) 1–7, https://doi.org/10.1016/j.peptides.2015.05.009. Epub 2015 Jun 3. PMID: 26048090.
[40] S.B. Petersen, L.G. Nielsen, U.L. Rahbek, M. Guldbrandt, D.J. Brayden, Colonic absorption of salmon calcitonin using tetradecyl maltoside (TDM) as a permeation enhancer, Eur. J. Pharm. Sci. 48 (4–5) (2013 Mar 12) 726–734, https://doi.org/10.1016/j.ejps.2013.01.009. Epub 2013 Jan 23. PMID: 23354154.
[41] Y. Narkar, R. Burnette, R. Bleher, R. Albrecht, A. Kandela, J.R. Robinson, Evaluation of mucosal damage and recovery in the gastrointestinal tract of rats by a penetration enhancer, Pharm. Res. 25 (1) (2008 Jan) 25–38, https://doi.org/10.1007/s11095-007-9509-8. Epub 2007 Dec 27. PMID: 18161013.
[42] X. Wang, S. Maher, D.J. Brayden, Restoration of rat colonic epithelium after in situ intestinal instillation of the absorption promoter, sodium caprate, Ther. Deliv. 1 (1) (2010 Jul) 75–82, https://doi.org/10.4155/tde.10.5. PMID: 22816121.
[43] D.J. Brayden, S. Maher, B. Bahar, E. Walsh, Sodium caprate-induced increases in intestinal permeability and epithelial damage are prevented by misoprostol, Eur. J. Pharm. Biopharm. 94 (2015 Aug) 194–206, https://doi.org/10.1016/j.ejpb.2015.05.013. Epub 2015 May 27. PMID: 26026287.
[44] C. Twarog, K. Liu, P.J. O'Brien, K.A. Dawson, E. Fattal, B. Illel, D.J. Brayden, A head-to-head Caco-2 assay comparison of the mechanisms of action of the intestinal permeation enhancers: SNAC and sodium caprate (C_{10}), Eur. J. Pharm. Biopharm. 152 (2020 Jul) 95–107, https://doi.org/10.1016/j.ejpb.2020.04.023. Epub 2020 May 6. PMID: 32387703.
[45] T.W. Leonard, J. Lynch, M.J. McKenna, D.J. Brayden, Promoting absorption of drugs in humans using medium-chain fatty acid-based solid dosage forms: gipet, Expet Opin. Drug Deliv. 3 (5) (2006 Sep) 685–692, https://doi.org/10.1517/17425247.3.5.685. PMID: 16948563.
[46] W. Shin, Z. Su, S.S. Yi, H.J. Kim, Single-cell transcriptomic mapping of intestinal epithelium that undergoes 3D morphogenesis and mechanodynamic stimulation in a gut-on-a-chip, iScience 25 (12) (2022 Nov 8) 105521, https://doi.org/10.1016/j.isci.2022.105521. PMID: 36425760; PMCID: PMC9678734.
[47] K. Wang, Y. Wang, J. Han, Z. Liang, W. Zhang, X. Li, J. Chen, L. Wang, Biofabrication and simulation techniques for gut-on-a-chip, Biofabrication 17 (2) (2025 Mar 20), https://doi.org/10.1088/1758-5090/adb7c1. PMID: 39965538.